Cellular Microbiology (2007) **9**(3), 790–803
doi:10.1111/j.1462-5822.2006.00832.x
First published online 28 November 2006

A FRET analysis to unravel the role of cholesterol in Rac1 and PI 3-kinase activation in the InlB/Met signalling pathway

Stéphanie Seveau,[1,2] To N. Tham,[1] Bernard Payrastre,[3] Adam D. Hoppe,[2] Joel A. Swanson[2]* and Pascale Cossart[1]*

[1]*Institute Pasteur, Unité des Interactions Bactéries-Cellules, Paris, F-75015; Inserm, U604, Paris, F-75015; INRA, USC2020, Paris F-75015, France.*
[2]*Department of Microbiology and Immunology, University of Michigan Medical School, Ann Arbor, MI 48109-0620, USA.*
[3]*Inserm, U563, Departement d'Oncogenèse et Signalisation dans les Cellules Haematopoietiques, Centre Hospitalier Universitaire Purpan, 31059 Toulouse, France.*

Summary

The signalling pathway for the hepatocyte growth factor receptor, Met/HGF-R, is hijacked by the bacterial surface protein InlB to induce *Listeria monocytogenes* entry into non-phagocytic cells. We previously showed that *Listeria* invades host cells by interacting with specialized microdomains of the host plasma membrane called lipid rafts. In this study, we analysed in living cells signalling events that are crucial for *Listeria* entry using a fluorescence resonance energy transfer-based microscopic method. Phosphoinositide (PI) 3-kinase activity and Rac1 signalling induced by *Listeria* interacting with epithelial cells were monitored as well as signalling induced by soluble InlB and the Met natural ligand HGF. We found that InlB and HGF induced similar kinetics of PI 3-kinase and Rac1 activation. PI 3-kinase activation was upstream and independent of Rac1 activation. Cholesterol-depletion experiments were performed to address the role of lipid rafts in Met signalling. The amount of 3′-phosphoinositides produced by PI 3-kinase was not affected by cholesterol depletion, while their membrane dynamic was cholesterol-dependent. Rac1 activation, downstream from PI 3-kinase, was cholesterol-dependent suggesting that the spatial distribution of 3′-phosphoinositides within membrane microdomains is critical for Rac1 activation and consequently for F-actin assembly at bacterial entry site.

Received 10 June, 2006; revised 30 August, 2006; accepted 31 August, 2006. *For correspondence. E-mail jswan@umich.edu; Tel. (+1) 734 647 72 93; Fax (+1) 734 764 3562.

Introduction

Listeria monocytogenes is a food-borne pathogen that infects humans and various animal species, causing severe diseases (Vazquez-Boland *et al*., 2001). In the host, *L. monocytogenes* invades and replicates in various cell types (Lecuit *et al*., 2001). *In vitro* studies have shown that the *L. monocytogenes* surface protein InlB is sufficient to induce bacterial entry into non-phagocytic cells (Dramsi *et al*., 1995; Cossart and Sansonetti, 2004). InlB-mediated bacterial internalization involves membrane microdomains, also called lipid rafts, and the clathrin endocytic machinery (Seveau *et al*., 2004; Veiga and Cossart, 2005). At its N-terminus, InlB contains leucine-rich repeats (LRR) which are sufficient to induce bacterial entry. In the C-terminus, GW motifs mediate non-covalent anchorage to the bacterial cell wall. As a consequence, some InlB can be released in the extracellular environment and can act as a soluble factor affecting host cell signalling and inducing membrane ruffling (Bierne and Cossart, 2002).

The hepatocyte growth factor receptor (Met/HGF-R) was identified as the major receptor for InlB responsible for *L. monocytogenes* entry into non-phagocytic cells, as well as for cell scattering and membrane ruffling induced by soluble InlB (Shen *et al*., 2000). Met is a heterodimeric tyrosine kinase receptor that plays a crucial role in organ morphogenesis (Santos *et al*., 1994; Schmidt *et al*., 1995; Birchmeier and Gherardi, 1998).

Major challenges are to explain how InlB subverts Met functions to induce bacterial entry and to determine if InlB and HGF are identical in the signals they generate through Met. InlB and HGF are dissimilar in sequence and structure, and bind to different sites on Met (Shen *et al*., 2000). The N-terminus of InlB binds to Met, and its GW motifs interact with glycosaminoglycans that are known to play a role in HGF-induced Met activation (Jonquieres *et al*., 2001; Banerjee *et al*., 2004). Investigations of Met signalling showed that HGF and InlB share common

effectors (Bierne *et al*., 2000; 2005; Bierne and Cossart, 2002; Sun *et al*., 2005); equal concentrations of InlB and HGF induce a similar level of Met phosphorylation and similar rates of Met endocytosis (Li *et al*., 2005). However, InlB induces a less sustained phosphorylation of Met (Shen *et al*., 2000) and a more pronounced activation of the Ras-MAP kinase pathway (Copp *et al*., 2003).

Membranes are compartmentalized into microdomains of distinct biochemical and physical properties. Among these microdomains, lipid rafts were defined as liquid-ordered, cholesterol- and glycolipid-enriched assemblies (Rajendran and Simons, 2005). Functionally, lipid rafts participate in signalling (Golub *et al*., 2004). Although roles for lipid rafts in HGF-Met signalling have not been reported, we demonstrated that InlB-induced *L. monocytogenes* entry and InlB-induced membrane ruffling involve a lipid raft-dependent signalling cascade leading to F-actin remodelling (Seveau *et al*., 2004).

This work compared Met signalling induced by InlB and HGF and investigated in living cells the role of cholesterol in signalling events that are critical for *L. monocytogenes* entry. A fluorescence resonance energy transfer (FRET)-based microscopic method (Hoppe *et al*., 2002) was used to visualize and to quantify phosphoinositide (PI) 3-kinase activity and Rho-family GTPase activation upon entry of a *Listeria innocua* strain that expresses InlB or stimulation by soluble InlB and HGF. Our results demonstrate that membrane organization is critical for the signalling induced by 3′-phosphoinositides resulting from PI 3-kinase activation.

Results

Visualization of PI 3-kinase and Rac1 activation at bacterial entry sites

Activation of PI 3-kinase and Rac1 was analysed in living cells using FRET-based microscopic methods (Hoppe *et al*., 2002). Analysis of PI 3-kinase activation was based on the detection of its lipid products $PI(3,4)P_2$ and $PI(3,4,5)P_3$. The serine/threonine kinase Akt translocates from the cytosol to the membrane, where the Akt pleckstrin homology domain specifically interacts with $PI(3,4)P_2$ and $PI(3,4,5)P_3$ (Haugh *et al*., 2000; Osaki *et al*., 2004). The quantification of FRET between two coexpressed fluorescent chimeras of the Akt pleckstrin homology domain, YFP-AktPH and CFP-AktPH, was used as readout of PI 3-kinase activity. The fluorescent chimeras are too dispersed in the cytosol to undergo FRET. Upon PI 3-kinase activation, the concentration of the fluorescent AktPH chimeras should increase at the plasma membrane, consequently leading to an increase in the FRET signal. Vero cells expressing CFP-AktPH and YFP-AktPH were imaged on the microscope stage in the presence of InlB-expressing bacteria. To study the InlB-dependent bacterial entry specifically, we used the normally non-invasive bacterial strain, *L. innocua,* that gained invasiveness solely through the expression of InlB from a plasmid (Braun *et al*., 1999). Because a very low percentage of bacteria induce host cell signalling and undergo entry, the experimental conditions where optimized to record signalling events on the microscope stage. A first step of centrifugation was performed to increase the number of bacteria interacting with the cells. This was done at 4°C to prevent internalization during centrifugation. A second step consisted in imaging the cells at room temperature (25°C) to slow the process of internalization, which takes only 5 min at 37°C. Phase-contrast and fluorescence images, corresponding to CFP (I_D), YFP (I_A) and FRET (I_F) fluorescence, were acquired every 20 s from cells on the microscope stage. FRET was reported as $(E_A + E_D)/2$ value, a correction for variability in fluorescent chimera expression within and among cells (Hoppe and Swanson, 2004) (see *Experimental procedures*). As shown in Fig. 1A, PI 3-kinase was transiently activated as soon as 2 min after bacterial contact, with a signal disappearing in less than 15 min (Movie 1A and B). Surprisingly, by an unknown mechanism, AktPH chimeras were often concentrated along dynamic phase-bright structures that resembled tubular vesicles (Movie 1A and B).

To visualize Rac1 activation, Vero cells were co-transfected with plasmids encoding YFP-Rac1 and CFP-PBD. This assay was based on the fact that in its active GTP-bound state, Rac1 forms a bimolecular complex with the p21-binding domain of PAK1 (PBD) (Benard *et al*., 1999). The proximity of fluorophores within the YFP-Rac1/CFP-PBD complex allowed FRET stoichiometry measurements, as previously described (Hoppe and Swanson, 2004). In these experiments FRET measured the fraction of active fluorescent GTPase expressed in the cell (see *Experimental procedures*). After pre-incubation with InlB-expressing bacteria at low temperature to prevent entry (see *Experimental procedures*), cells were placed on the microscope stage and images were acquired every 20 s. As shown in Fig. 1B, Rac1 was activated at the region of the plasma membrane interacting with the bacteria (see Movie 2A and B). However, quantitative comparisons of PI 3-kinase and Rac1 activation during multiple entry events were not feasible because a very low percentage of bacteria induced host cell signalling and their uptake, in addition, it was difficult to determine precisely when bacteria contacted the plasma membrane and when they were internalized. In addition, the time delay between initial bacteria–cell interaction and the generation of signal was highly variable. Thus to further understand the mechanisms underlying InlB/Met-dependent signalling, we decided to analyse and compare the Rac1 and PI 3-kinase signalling induced by soluble InlB with that induced by HGF.

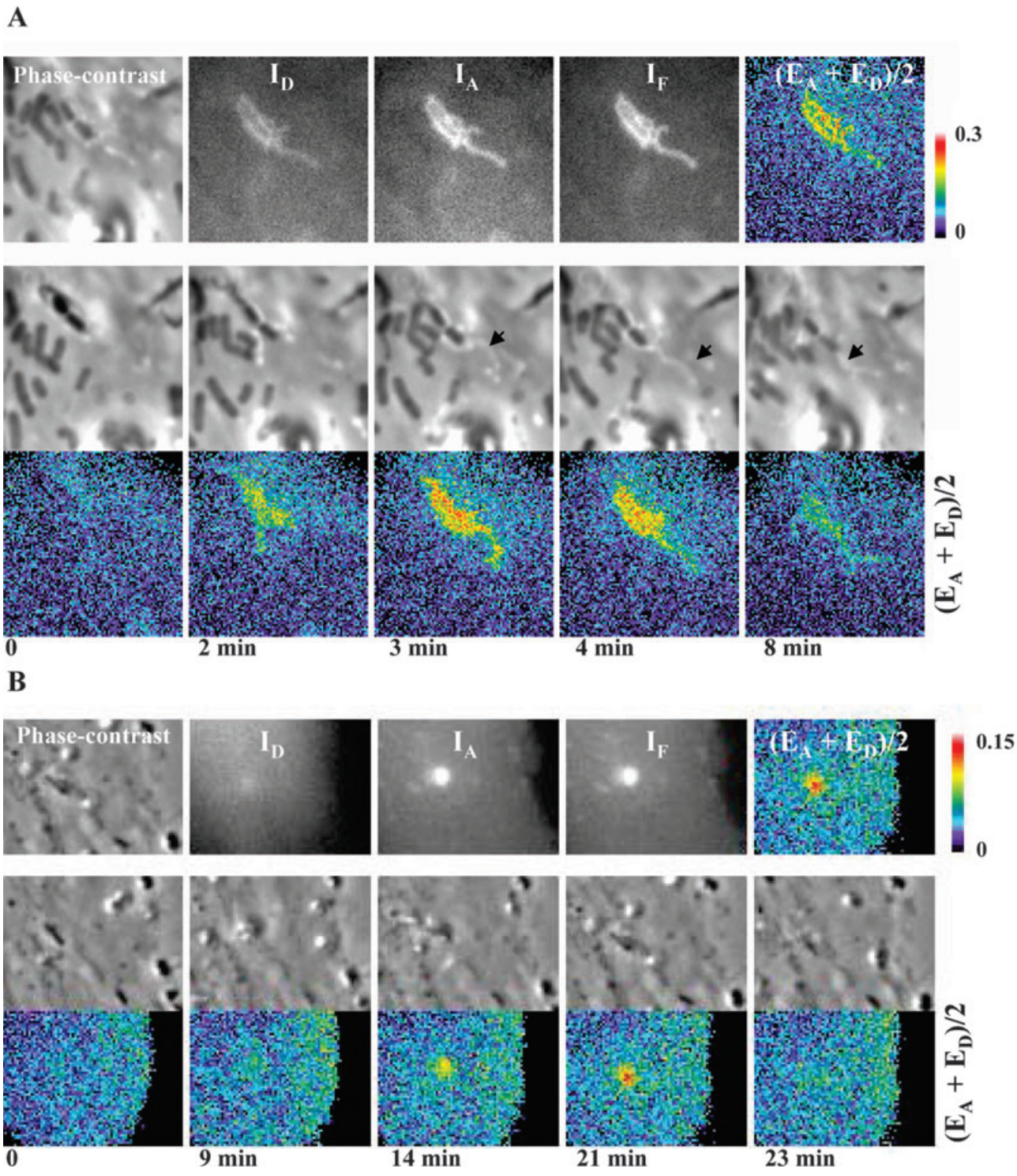

Visualization of membrane ruffling induced by soluble InlB and HGF

Initial comparisons of membrane ruffling induced by InlB and HGF in Vero cells allowed to determine the delay between addition of soluble ligand and the formation of actin-rich membrane ruffles, as well as the duration of membrane ruffling. Membrane ruffling was observed by phase-contrast microscopy, and F-actin remodelling within ruffles was visualized in cells coexpressing YFP-actin and CFP. Fluorescence and phase-contrast images corresponding to YFP-actin (I_Y) and CFP (I_C) were

Fig. 1. Visualization of PI 3-kinase and Rac1 activation at bacterial entry sites using FRET stoichiometry.
A. Vero cells expressing YFP-AktPH plus CFP-AktPH were incubated with a *L. innocua* strain expressing InlB. Phase-contrast and fluorescence images (I_A, I_D, I_F) were collected every 20 s for 30 min. Quantification of FRET between fluorescent chimeras was achieved as described in *Experimental procedures* and was expressed as $(E_A + E_D)/2$ at each pixel of the processed FRET image. The pseudocolour bar indicates the range of $(E_A + E_D)/2$ values. The figure shows collected and processed images at different times after the start of acquisition. PI 3-kinase was activated at the membrane surrounding the bacterium and along phase-bright extensions resembling tubular vesicles, indicated with the black arrows (Movie 1A and B).
B. Vero cells expressing YFP-Rac1 plus CFP-PBD were incubated with a *L. innocua* strain expressing InlB. Phase-contrast and fluorescence images (I_A, I_D, I_F) were collected every 20 s for 30 min. Quantification of FRET between fluorescent chimeras was achieved as described in *Experimental procedures* and was expressed as the fraction of activated Rac1 (*G* value) in the processed FRET images. The colour bar indicates the range of *G* values. The figure shows representative collected and processed images at different times after the start of acquisition. Rac1 was activated at the membrane surrounding the bacterium (Movie 2A and B).

acquired every 20 s for 30 min. A ratio image was obtained by dividing, pixel by pixel, I_Y by I_C. This processing allowed to correct the fluorescence images for differences in cell thickness. At 3 min after the start of recording (T_0), cells were activated with 1.25 nM InlB or HGF. As shown in Fig. 2, 3 min after Met activation large actin-rich membrane ruffles were formed (Movie 3A and B). Analysis of at least 10 movies in each condition showed that membrane ruffling started 1 min after stimulation by InlB or HGF, and large ruffles were formed after 3 min. The total duration of membrane ruffling was 16.1 ± 1.7 min for InlB and 15.2 ± 1.9 min for HGF. Cells were cholesterol-depleted with 10 mM methyl-β-cyclodextrin (MβCD) and assayed for membrane ruffling. In agreement with our previous report (Seveau *et al.*, 2004), formation of F-actin-rich membrane ruffles by InlB and HGF was totally abrogated in cholesterol-depleted cells (Fig. 2).

InlB and HGF induce similar kinetics of PI 3-kinase activation

The kinetics of PI 3-kinase activation by soluble InlB and HGF were monitored microscopically in Vero cells

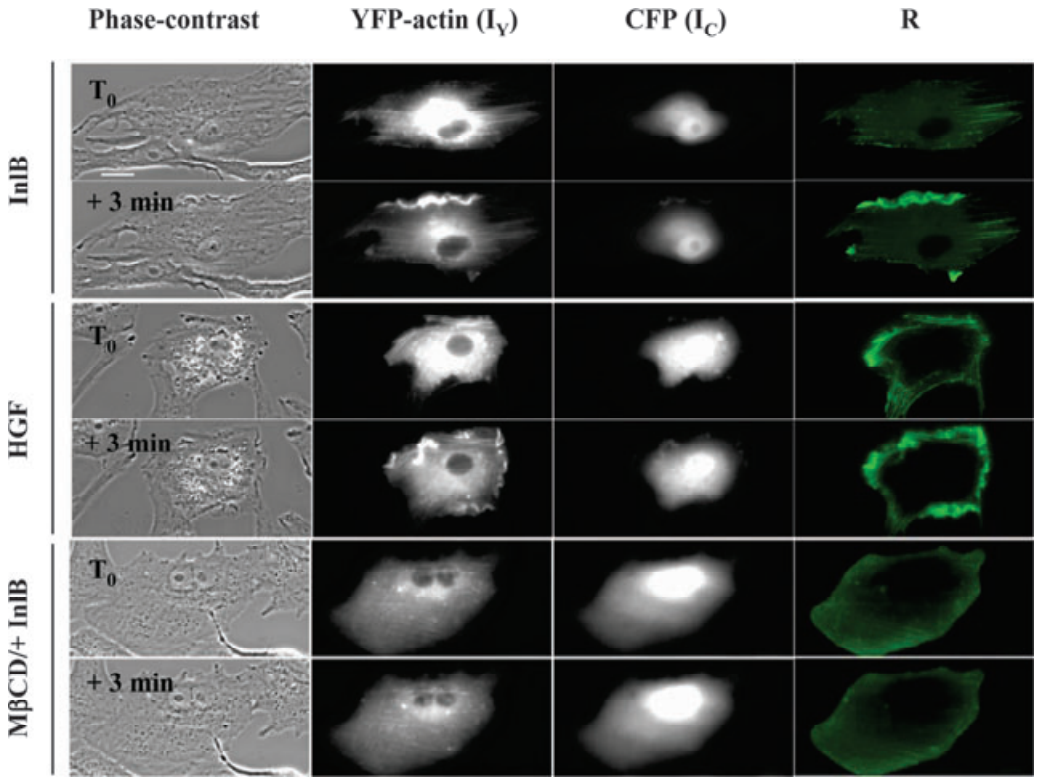

Fig. 2. Visualization of membrane ruffling induced by InlB and HGF. Vero cells were co-transfected with plasmids encoding CFP and YFP-actin. Phase-contrast and fluorescence images (I_Y, I_C) of control and cholesterol-depleted cells were recorded every 20 s for 30 min. InlB (1.25 nM) or HGF (1.25 nM) was added 3 min after the start of imaging (T_0). Two time points are presented (T_0, $T_0 + 3$ min). Scale bar = 20 μm (Movie 3A and B).

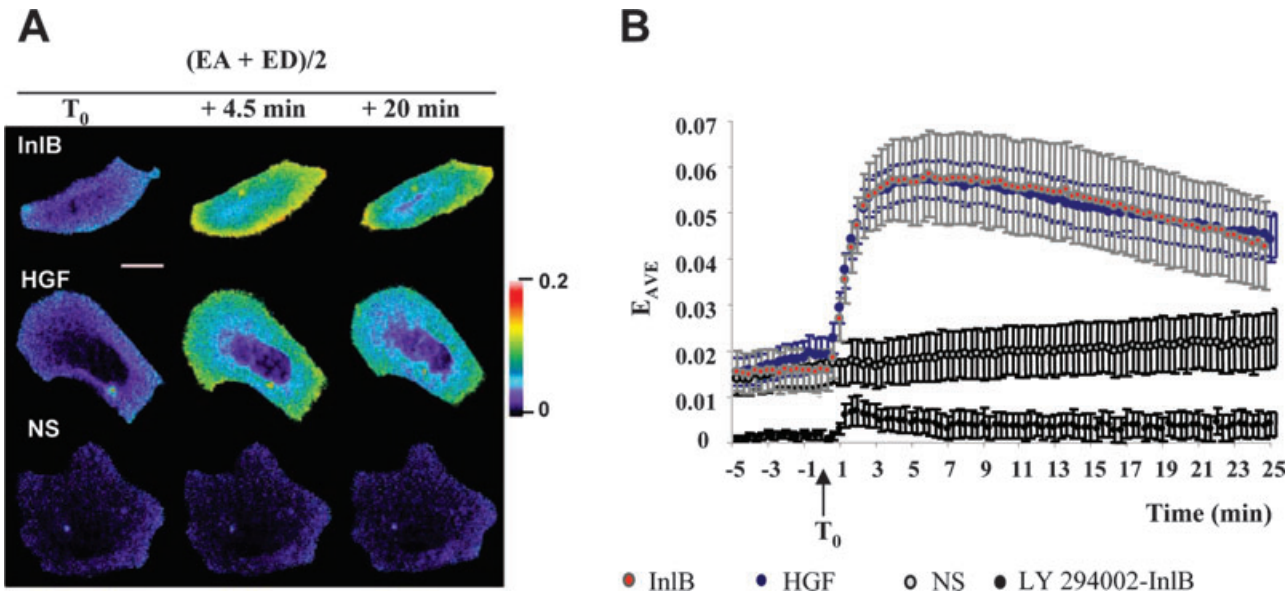

Fig. 3. InlB and HGF induce similar kinetics of PI 3-kinase activation. Transiently transfected Vero cells were placed on the microscope stage at 37°C and image series were collected every 20 s for 30 min. InlB or HGF was added 4.5 min after the start of imaging.
A. Processed FRET images of cells expressing YFP-AktPH plus CFP-AktPH, stimulated with 1.25 nM InlB or HGF and of an unstimulated cell (NS). Three time points are presented (0, 4.5 and 20 min after stimulation).
B. PI 3-kinase activity was determined from the average $(E_A + E_D)/2$ value (E_{AVE}) from at least 10 cells in each condition tested. Control, unstimulated cells (grey), cells stimulated with InlB (black, red) or with HGF (blue). Scale bar = 20 μm. The colour bars represent the range of $(E_A + E_D)/2$ values (Movie 4A–C). Error bars are the SEM of average values for each point. The baseline levels of activation of stimulated cells and of the control unstimulated cells differed slightly from cell to cell (A) but on the average, as presented on the graph (B), they were the same (except for cells pretreated with LY294002).

expressing YFP-AktPH and CFP-AktPH. Phase-contrast and fluorescence images (I_A, I_D, I_F) were acquired every 20 s for 30 min. InlB or HGF (1.25 nM) was added 4.5 min after the start of imaging (T_0). Figure 3A shows FRET images of cells activated with InlB or HGF, and of control unstimulated (NS) cells at different points of the sequence (T_0, +4.5 min, +20 min) (Movie 4C). InlB and HGF induced similar spatial recruitment of AktPH over the entire plasma membrane. In the unstimulated cells (NS), the FRET level remained low over the 20 min period. To quantify the kinetics of AktPH membrane recruitment, FRET signals from at least 10 cells were expressed as the mean $(E_A + E_D)/2$ value (E_{AVE}) (Fig. 3B). In unstimulated cells expressing CFP-AktPH and YFP-AktPH, the FRET levels remained constant and low (grey trace), indicating that baseline levels of 3′-phosphoinositides were low and that imaging over this time period did not affect FRET signals. Addition of InlB or HGF to cells expressing CFP-AktPH and YFP-AktPH increased the AktPH membrane recruitment within 30 s, indicated as increased E_{AVE}. The recruitment of AktPH reached a maximum after 4 min of stimulation and remained constant for about 5 min before slowly decreasing (red and blue traces). InlB and HGF induced similar kinetics of AktPH membrane recruitment. To confirm that the assay was indeed a read-out of PI 3-kinase activation, cells were pre-incubated with the PI 3-kinase inhibitor LY294002 before measuring responses to InlB and HGF. Before stimulation, the baseline level of FRET was diminished compared with control cells (black trace), indicating a low level of PI 3-kinase activation in cells without inhibitor prior to stimulation by InlB or HGF. Addition of InlB to LY294002-inhibited cells induced only a minor increase in E_{AVE}. FRET signals were not affected by the presence of 1/2000 dilution of DMSO that was used as a solvent for LY294002 (data not shown). Acquired and calculated FRET images after 4.5 min of stimulation with InlB are presented as Fig. S1 (see also Movie 4A and B).

InlB and HGF induce similar kinetics of Rac1 activation

Rho-family GTPase activation induced by InlB and by HGF was monitored in Vero cells co-transfected with plasmids encoding YFP-Rac1 and CFP-PBD. Figure S2 shows the phase-contrast, the fluorescence images (I_A, I_D, I_F) and the FRET quantification of active Rac1 (G) 1 min after stimulation with InlB. The activation of Rac1 was more pronounced at the cell periphery where membrane ruffles were formed (Movie 5A and B). To determine the kinetics of Rac1 activation in multiple cells, *G* was expressed as a mean value from at least 10 cells at each

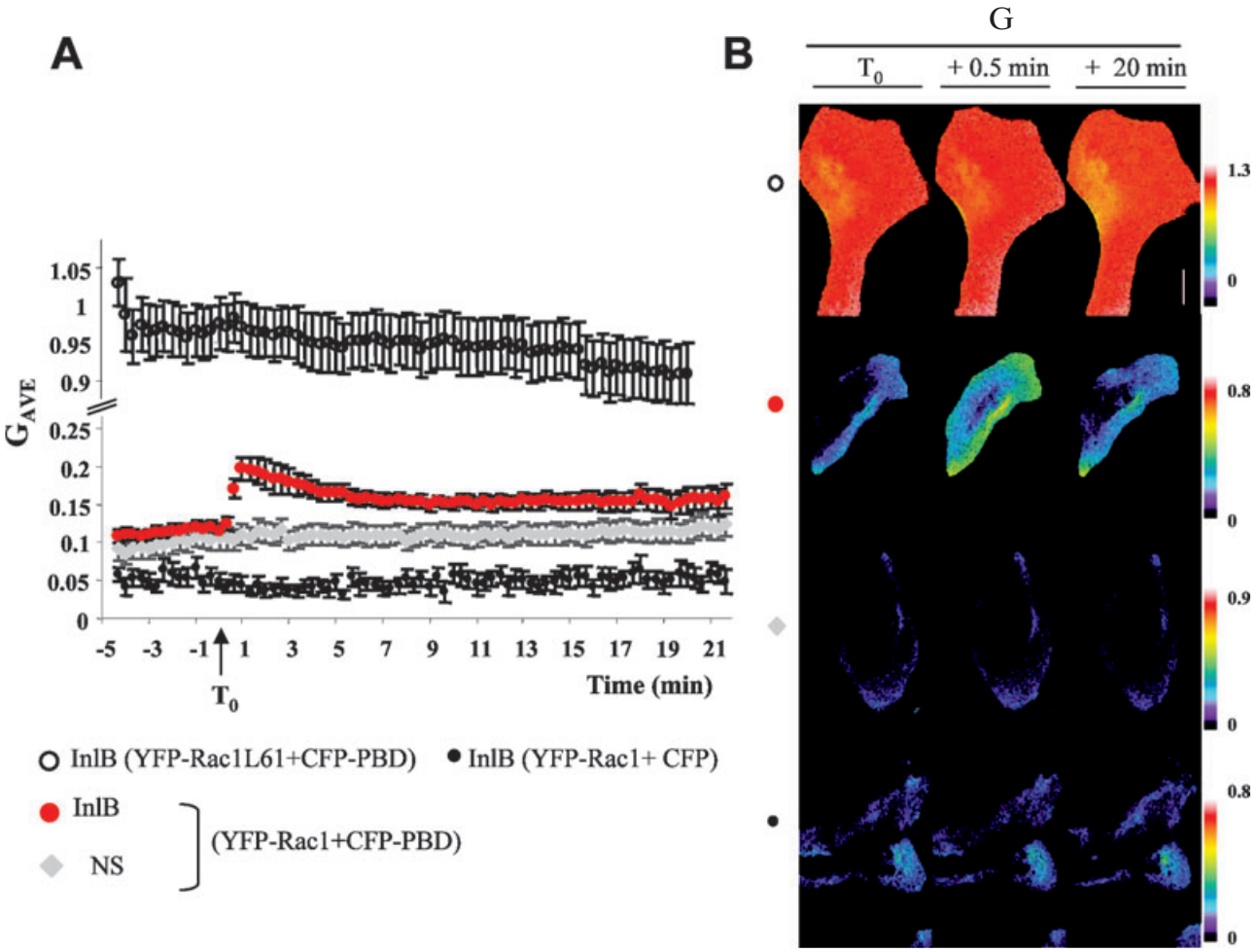

Fig. 4. Kinetics of Rac1 activation quantified by FRET stoichiometry. Transiently transfected Vero cells were placed on the microscope stage at 37°C and image series were collected every 20 s for 30 min. For the stimulated cells, 5.7 nM InlB was added 4.5 min after the start of imaging.
A. Rac1 activation over at least 10 cells was averaged and the results were expressed as the mean *G* value (G_{AVE}) ± SEM for each condition tested. Various combinations of fluorescent chimeras were expressed in Vero cells, YFP-Rac1 plus CFP (black), YFP-Rac1 plus CFP-PBD (grey, orange), YFP-Rac1L61 plus CFP-PBD (open circle). Cells were stimulated with InlB (black, orange, open circle), or not (grey).
B. Representative examples of processed FRET images corresponding to the kinetics presented in (B) at three time points (T_0, +0.5 min, +20 min). Scale bar = 20 μm. Colour bars represent the range of *G* values (Movie 5A–C).

time point (Fig. 4A). A background FRET value of 5% was observed in control cells expressing YFP-Rac1 and CFP (black trace). In unstimulated cells expressing YFP-Rac1 and CFP-PBD, Rac1 activation remained constant over the 30 min of recording, reflecting a constitutive level of 5% of YFP-Rac1 activation (after background correction, grey trace). In cells expressing the constitutively active form of Rac1 (YFP-Rac1L61) and CFP-PBD, more than 90% of the YFP-Rac1L61 molecules were measured to be activated and, as expected, this value was not affected by InlB stimulation (open circles). The addition of InlB to cells expressing YFP-Rac1 and CFP-PBD resulted in the activation of Rac1 within 30 s, reaching a maximum of 15% after 1 min. YFP-Rac1 activation remained maximal for up to 40 s then decreased to its baseline level after 5 min. FRET images corresponding to different time points (T_0, +0.5, +20 min) of the kinetics are shown in Fig. 4B (see also Movie 5C). We then compared InlB and HGF, as shown in Fig. 5A, InlB and HGF induced similar kinetics of Rac1 activation. The same experiments were performed using cells coexpressing YFP-Cdc42 plus CFP-PBD and no activation of Cdc42 was observed (data not shown). These results are in accordance with previous observations that Rac1 is critical for bacterial entry and membrane ruffling and that the expression of the Cdc42 dominant negative form Cdc42(N17) in Vero cells had no effect on InlB-dependent bacterial entry and membrane ruffling (Bierne *et al.*, 2001; 2005).

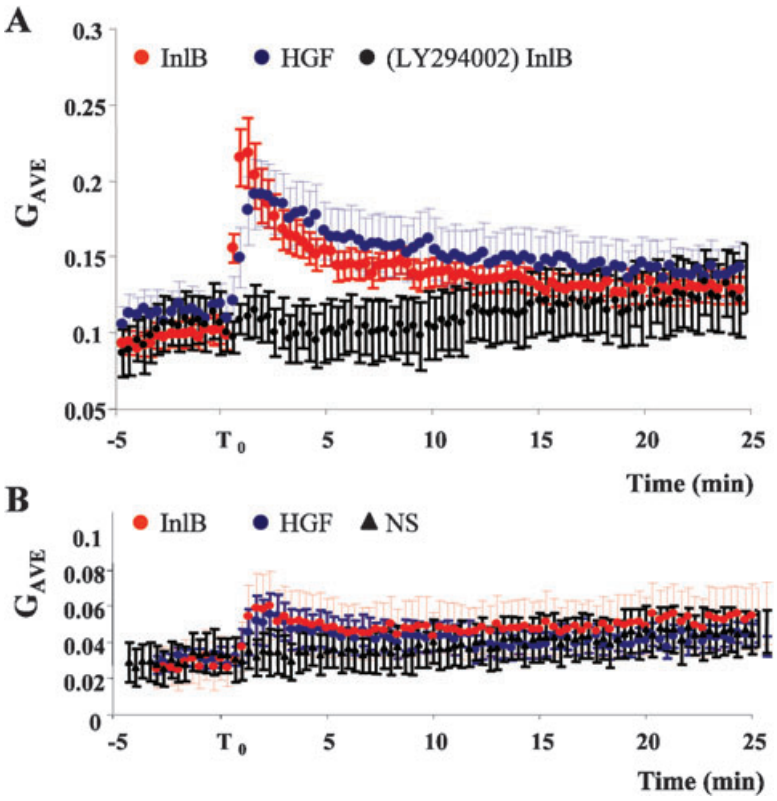

Fig. 5. InlB and HGF induce similar kinetics of Rac1 activation, by a PI 3-kinase- and cholesterol-dependent process. Vero cells coexpressing YFP-Rac1 plus CFP-PBD were placed on the microscope stage at 37°C and were imaged for FRET stoichiometry.
A. Kinetics of Rac1 activation in cells stimulated with 1.25 nM InlB (red, black) or HGF (blue) 4.5 min after the start of imaging. To assess the role of PI 3-kinase in Rac1 activation, cells were pre-incubated with PI 3-kinase inhibitor (LY294002) before FRET stoichiometric imaging (black).
B. To assess the role of cholesterol in Rac1 activation, cells were cholesterol-depleted with 10 mM MβCD before FRET stoichiometric imaging. Rac1 activation over at least 10 cells was averaged and the results were expressed as the mean *G* value (G_{AVE}) ± SEM for each condition tested. Control, unstimulated (NS) cells are presented in black, cells activated by InlB or by HGF are presented in red and blue respectively.

Rac1 activation occurs downstream from PI 3-kinase and is cholesterol-dependent

To assess if Rac1 activation by InlB was downstream from PI 3-kinase, as reported for HGF (Royal *et al*., 2000), cells were pre-incubated with the PI 3-kinase inhibitor, LY294002 (25 μM) for 30 min, before being assayed. PI 3-kinase inhibition completely abrogated Rac1 activation induced by InlB (Fig. 5A). The same results were obtained with cells stimulated with HGF (data not shown). Rac1 activation was not affected by the presence of 1/2000 dilution of DMSO that was used as a solvent for LY294002 (data not shown). We previously demonstrated that F-actin polymerization during InlB/Met-dependent *L. monocytogenes* entry and during membrane ruffling requires lipid raft integrity (Fig. 2, Seveau *et al*., 2004). Because Rho-family GTPases are known to be regulators of the actin cytoskeleton, we analysed if the defect of F-actin polymerization observed in cholesterol-depleted cells was due to a defect in Rac1 activation. Cells expressing YFP-Rac1 and CFP-PBD were cholesterol-depleted with 10 mM MβCD and were imaged in the absence of MβCD. As shown in Fig. 5B, InlB or HGF induced very low levels of Rac1 activation in cholesterol-depleted cells, similar to signals measured from unstimulated cells (NS). The baseline level of Rac1 activation was also low in cholesterol-depleted cells (Fig. 5B) compared with control non-depleted cells (Fig. 5A). We verified that cholesterol depletion did not affect the measurement of FRET. More precisely, the optical properties of the fluorescent proteins and the FRET signals from the constitutively active form of Rac1 (Rac1Q61L-YFP) and PBD-CFP were similar in cholesterol-depleted cells and control cells (data not shown). In conclusion, cholesterol depletion reduced both the constitutive baseline level of Rac1 activation and Rac1 activation induced by InlB and HGF.

PI 3-kinase and Akt activation do not require membrane cholesterol

We next asked if the diminished Rac1 activation was a consequence of a decreased PI 3-kinase activity. We quantified PI 3-kinase activity using biochemical measurements of the cellular phosphoinositides, before and after InlB stimulation, on control, non-depleted and on cholesterol-depleted cells. As shown in Fig. 6A and Fig. S3, cholesterol depletion did not affect the amount of the PI 3-kinase lipid products PI(3,4,5)P_3 and PI(3,4)P_2, or of the phosphoinositides PI(3)P, PI(4)P and PI(4,5)P_2. To confirm that PI 3-kinase activity was not affected in cholesterol-depleted cells, we analysed the activation of its downstream target Akt. Following its membrane recruitment through the pleckstrin homology domain, Akt was reported to be phosphorylated at the plasma membrane (Vanhaesebroeck and Alessi, 2000). Cells were

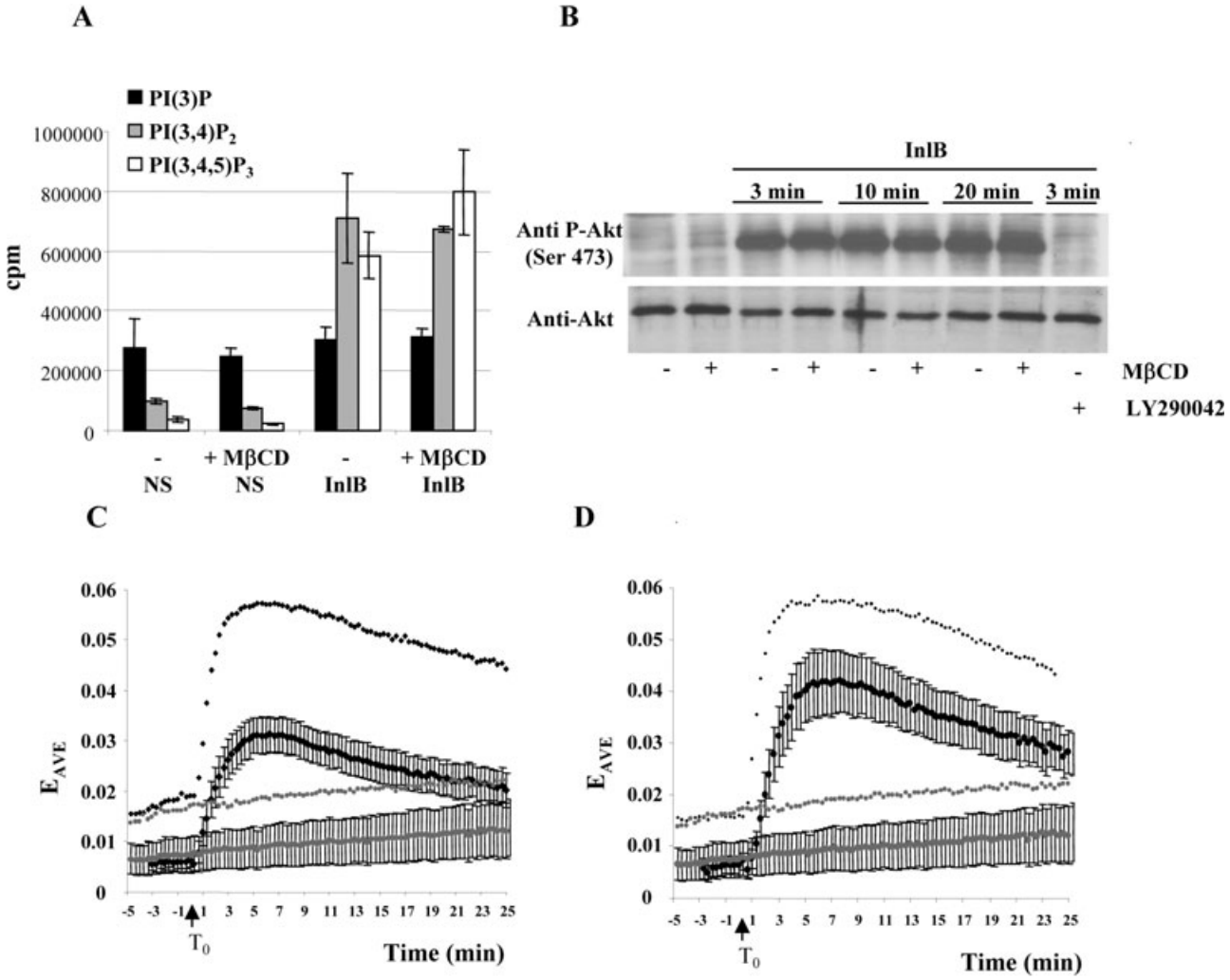

Fig. 6. PI 3-kinase activity and Akt phosphorylation by InlB and HGF are independent of lipid raft integrity.
A. Vero cells were pre-incubated with ^{32}Pi, and were cholesterol-depleted, or not (–), with 10 mM MβCD. After washes, cells were stimulated, or not (NS), with InlB for 2 min at room temperature. Phosphoinositides were then isolated and quantified by HPLC as described in *Experimental procedures*. Results were normalized according to the total amount of phospholipids present in each sample. Average ± SEM of two independent experiments are presented in cpm.
B. Western blotting of Phospho-Akt (Ser 473) and Akt on total cell extracts of control and cholesterol-depleted cells stimulated with 2 nM InlB for various times (0, 3 min, 10 min, 20 min). To demonstrate that Akt phosphorylation occurred downstream of PI 3-kinase, PI 3-kinase was inhibited by LY294002 and then cells were stimulated for 3 min by InlB.
C and D. FRET stoichiometry as a tool to investigate membrane microdomains in living cells. Vero cells expressing YFP-AktPH plus CFP-AktPH were cholesterol-depleted using 10 mM MβCD for 30 min. After washes, cells were placed on the microscope stage at 37°C and image series were collected every 20 s for 30 min. Cells were stimulated (black) or not (grey) by 1.25 nM InlB (C) or HGF (D) at T_0. The results were expressed as E_{AVE} of at least 10 cells in each condition tested (traces with error bars). For comparison with control non-depleted cells, results from Fig. 5 are shown as traces without error bars.

cholesterol-depleted, or not, and stimulated for 3, 10 and 20 min with InlB, the phosphorylation of endogenous Akt (Serine 473) was analysed by Western blot analysis of total cell extracts (Fig. 6B). No difference in Akt phosphorylation was detectable between cholesterol-depleted and non-depleted cells after stimulation with InlB, indicating that cholesterol depletion did not affect Akt targeting to the plasma membrane and its activation.

FRET measurements to investigate membrane microdomain organization in living cells

In these experiments FRET analyses were aimed to measure the proximity between fluorescent chimeras. The amplitude of FRET signals from cells coexpressing YFP-AktPH and CFP-AktPH reflected the global membrane content of 3′-phosphoinositides, as well as the possible

membrane clustering of the fluorescent molecules within microdomains. To determine if Met signalling cascade occurs within membrane microdomains, FRET between the AktPH fluorescent chimeras was compared between control and cholesterol-depleted cells. This comparison was possible because cholesterol depletion did not decrease the global membrane content of 3′-phosphoinositides on InlB-stimulated cells (Fig. 6A), or the membrane recruitment and activation of the endogenous Akt (Fig. 6B). Accordingly, if 3′-phosphoinositides were clustered within membrane microdomains, microdomain disruption by cholesterol depletion should diminish the amplitude of the FRET signals in response to stimulation. Transfected Vero cells were cholesterol-depleted with 10 mM MβCD; cells were then washed and imaged in the absence of MβCD. InlB or HGF stimulation of cholesterol-depleted cells resulted in similar kinetics of FRET signals (black traces with error bars) compared with control non-depleted cells (grey diamonds, no error bars) (Fig. 6C and D). The kinetics and the slopes of increase and decrease of FRET signals were similar in cholesterol-depleted cells compared with non-depleted cells; however, the amplitudes of FRET signals were lower in cholesterol-depleted cells in accordance with our hypothesis. Also the localization of the FRET signals was similar on cholesterol-depleted and control non-depleted cells (data not shown). We verified that cholesterol depletion did not affect the measurement of FRET (data not shown). These results indicated a role for $PI(3,4)P_2$ and $PI(3,4,5)P_3$ in AktPH-chimeras clustering, presumably within lipid rafts.

Discussion

This study analysed Met/HGF-R signalling activated by the bacterial invasion protein InlB. PI 3-kinase and Rac1 are crucial signalling molecules required for bacterial invasion of host cells. Rac1 activation is known to induce the polymerization of actin at the entry site, while the precise role of PI 3-kinase was unknown. We addressed the spatiotemporal kinetics of PI 3-kinase and Rac1 activation induced by InlB in comparison with HGF, the Met natural ligand, using a FRET-based microscopic method (Hoppe *et al*., 2002). This study allowed us to establish the connection between PI 3-kinase and Rac1 signalling and to clearly identify the role of membrane cholesterol in Rac1 activation.

InlB functionally mimics HGF

PI 3-kinase and Rac1 activation induced by InlB-expressing *L. innocua* were visualized for the first time (Fig. 1A and B). Surprisingly, PI 3-kinase lipid products propagated from the phagocytic membranes along elongated phase-bright structures at the bacterial entry site (Fig. 1A). These tubular structures could correspond to membrane extensions originating from the *Listeria* vacuole, or to a tubular membrane network that fuses with *Listeria* vacuole. Quantification of Rac1 and of PI 3-kinase signalling during bacterial entry was not feasible, because it was not feasible to record in addition to cell signalling when the bacteria were fully internalized. For quantitative studies we instead analysed signalling induced by soluble InlB. Met activation by soluble InlB and by InlB expressed at the bacterial surface might not be equivalent but share common transducers such as PI 3-kinase and Rac1. Strikingly, although InlB and HGF are dissimilar in sequence and structure, and bind to different sites on Met (Shen *et al*., 2000), they induced similar kinetics of membrane ruffling (Fig. 2), PI 3-kinase (Fig. 3) and Rac1 (Fig. 5) activation.

Rac1 activation by InlB is dependent on PI 3-kinase

The precise role of PI 3-kinase in *Listeria* entry and in InlB-dependent membrane ruffling remained elusive. We demonstrated that PI 3-kinase activation was necessary for Rac1 activation (Fig. 5A) and the consequent F-actin remodelling. This result is in accordance with the observation that PI 3-kinase inhibition by LY294002 abrogated the formation of actin-rich membrane ruffles (Figs 2 and 5A) as previously observed (Ireton *et al*., 1999). There was no evidence of a feedback loop between Rac1 and PI 3-kinase, as observed in other systems (Genot *et al*., 2000), because Rac1 inhibition by cholesterol depletion (Fig. 5B) did not affect PI 3-kinase activity (Fig. 6A). We compared the time-courses for PI 3-kinase and Rac1 activation. Both were activated within 30 s of stimulation; Rac1 was downregulated after 1 min, while the 3′-phosphoinositide levels were still maximal (Figs 3 and 5A). In conclusion, Rac1 downregulation might occur independently of the level of PI 3-kinase lipid products. The signalling molecules that link PI 3-kinase activation to Rac1 are not yet identified. A possible candidate is the Rac exchange factor Dock 180, which contains a $PI(3,4,5)P_3$-binding domain (DHR-1) (Kiyokawa *et al*., 1998). We could not detect Cdc42 activation in Vero cells, consistent with the observations that Cdc42 activation by InlB and by HGF is cell type-dependent; Cdc42 and Rac1 are both activated in other cell types but not in Vero cells (Royal *et al*., 2000; Bierne *et al*., 2001; 2005).

Rac1 but not PI 3-kinase activity is cholesterol-dependent

We demonstrated that PI 3-kinase activity was insensitive to the level of membrane cholesterol and, consequently to lipid raft integrity (Fig. 6A). However, Rac1 activation

required membrane cholesterol and presumably also lipid rafts, although cholesterol-depletion experiments only indicate possible roles for lipid rafts. The strong decrease in Rac1 activation explains the defect in actin polymerization on cholesterol-depleted cells at the entry site and in membrane ruffles. Consistent with this conclusion, overexpression of a dominant negative form of Rac1 abrogated entry and membrane ruffling (Bierne *et al*., 2001). Although other studies have addressed the role of lipid rafts in Rac1 activation and in F-actin dynamics, this study addressed this question in living cells, combining quantitative, spatial and temporal studies. The constitutively active form of Rac1 (Rac1Q61L) was still localized at the plasma membrane on cholesterol-depleted cells, suggesting that cholesterol is required for Rac1 activation rather than for its membrane association (data not shown). In contrast to the results shown here, it was reported that cholesterol depletion did not affect Rac1 activation but abrogated the recruitment of Rac1-GTP to the plasma membrane (del Pozo *et al*., 2004). In agreement with our studies, it was reported that Rac1 activation was affected by cholesterol depletion (Pierini *et al*., 2003) and Rac1-GTP was reported to selectively localize in detergent-resistant membranes, indicating that Rac1 was activated within lipid rafts (Fujitani *et al*., 2005; Wysoczynski *et al*., 2005). Our results further indicate that the spatial distribution of 3′-phosphoinositides is crucial for downstream Rac1 activation (Fig. 6C and D).

FRET stoichiometry imaging to study membrane organization in microdomains

We utilized FRET imaging to study the distribution of phosphoinositides within the plasma membrane. FRET signals reflect the proximity of the fluorescent chimeras and consequently FRET signal from AktPH fluorescent chimeras reflects both the level of 3′-phosphoinositides and their possible concentration in membrane microdomains. As total phosphoinositide levels were not affected by cholesterol depletion (Fig. 6A), our results favour the hypothesis that the decrease in FRET on cholesterol-depleted cells was the consequence of membrane microdomain disorganization (Fig. 6). We cannot rule out the possibility that AktPH chimeras are not equally recruited at the membrane on cholesterol-depleted cells compared with control cells. However, endogenous Akt molecules were equally recruited and activated at the membrane (Fig. 6B), both processes proven to be dependent on the association to membrane 3′-phosphoinositides by the AktPH domains (Osaki *et al*., 2004). Our methodological approach indicates that cholesterol levels within the plasma membrane control the clustering of the AktPH chimeras, although we cannot rule out that other indirect effects of the MβCD drug also affect the FRET between the AktPH chimeras. A clear demonstration of the organization of the 3′-phosphoinositides and of the fluorescent chimeras within microdomains would require the direct observation of fluorescent signals in unperturbed living cells. Unfortunately, we are lacking of technological tools to perform such experiments. We hypothesized that the nanoscale distribution of PI 3-kinase products within the membrane appears determinant for Rac1 activation. In conclusion, a productive signalling cascade leading to Rac1 activation and F-actin polymerization appears to depend on whether or not Met signalling occurs within cholesterol-enriched membrane domains, while Akt activation is less sensitive to the integrity of membrane microdomains. It remains unknown how these two downstream signalling effectors of PI 3-kinase (Rac and Akt) are differentially regulated by their membrane microenvironment.

Does InlB elicit different signals from HGF to promote bacterial entry?

Because cellular uptake of bacteria is not the physiological function of Met, a fundamental question is how InlB/Met-dependent bacterial entry occurs. Consistent with the hypothesis that InlB mimics HGF, both induced identical patterns of PI 3-kinase and Rac1 activation. It was reported that addition of HGF to a *Listeria* strain lacking the expression of InlB (EGD Δ*InlB*) promoted invasion of Vero cells as efficiently as soluble InlB (Banerjee *et al*., 2004) and that soluble InlB promoted entry of other bacteria (Braun *et al*., 1998). InlB induces a less sustained phosphorylation of Met (Shen *et al*., 2000) and a more pronounced activation of the Ras-MAP kinase pathway (Shen *et al*., 2000; Copp *et al*., 2003). Whether or not these differences contribute to bacterial invasion and in particular to the hijacking of the endocytosis machinery (Veiga and Cossart, 2005) remains to be determined. These differences could also serve additional functions of InlB involved in other stages of pathogenesis. The different biological outcomes of Met activation in physiological and pathological contexts might be modulated by the combination of several parameters. Our results indicate that the localization of Met signalling effectors within lipid rafts determines the fate of the signalling cascade. In addition, several bacterial factors might modulate Met activation, such as Listeriolysin O, a secreted cholesterol-dependent toxin that has been shown to increase InlB-dependent *Listeria* internalization and to cluster lipid rafts (Dramsi and Cossart, 2003; Gekara *et al*., 2005). Listeriolysin O may magnify the formation of lipid rafts, increasing Rac1 activation at bacterial entry site. The next challenging issue is to study the cooperation between *Listeria* virulence factors in the regulation of Met/HGF-R signalling.

Experimental procedures

Reagents, mammalian cells, bacteria and constructs

Methyl-β-cyclodextrin, HGF and the PI 3-kinase inhibitor LY294002 were from Sigma-Aldrich. Purification of recombinant 6-His-tagged InlB was performed as previously described (Ireton *et al*., 1999). African green monkey kidney epithelial Vero cells (American Type Culture Collection; CCL-81) were cultured in DMEM glutamax (Gibco BRL) supplemented with 10% FBS. For microscopy, cells were seeded in coverslip bottom culture dishes (MatTek Corporation) 24 h before transfection. Cells were transiently transfected with Lipofectamin 2000 (Gibco BRL) following the manufacturer's instructions. For microscopic analyses, after 24–48 h of transfection, cells were incubated in a medium containing 150 mM NaCl, 5 mM KCl, 1 mM $MgCl_2$, 1 mM $CaCl_2$, 10 mM glucose, 20 mM Hepes pH 7.4 at 37°C. Construction of plasmids encoding YFP-Rac1, YFP-Cdc42, YFP-Rac1L61, YFP-Cdc42V12, CFP-PBD, YFP-AktPH and CFP-AktPH were described previously (Hoppe and Swanson, 2004), as was the construction of YFP-actin (Henry *et al*., 2004). To reduce the possibility of fluorescent protein-mediated dimerization (Zacharias *et al*., 2002), YFP-labelled GTPases and YFP-AktPH were made with monomeric citrine, CFP-PBD and CFP-AktPH were made with monomeric CFP. *L. innocua* transformed with pAT18pprot + LRRs-IR-InlB-SPA (BUG 1642) (Braun *et al*., 1999) were grown overnight at 37°C in brain–heart infusion agar (Difco) with 5 μg ml^{-1} erythromycin, diluted 10 times in brain–heart infusion, and cultured until OD_{600} = 0.8. Bacteria were then washed in culture medium and were added to Vero cells (10^8 bacteria per microscopy dish) and centrifuged at 4°C for 10 min at 1500 rpm before being imaged at room temperature.

Cholesterol depletion and LY294002 treatment

For cholesterol depletion, cells were washed twice with DMEM (without serum) and incubated at 37°C for 30 min with 10 mM MβCD in DMEM. Cells were then washed twice and assayed as described. The cholesterol levels before and after depletion were quantified by gas chromatography as described previously (Bodin *et al*., 2001); about 60% of total cholesterol was depleted. To inhibit PI 3-kinase, cells were incubated with 25 μM LY294002 (50 mM stock solution in DMSO) for 30 min at 37°C; cells were then assayed as described in the presence of LY294002.

Microscope equipment

Images were acquired with a motorized inverted fluorescence microscope (Axiovert 200I, Carl Zeiss MicroImaging) equipped with a temperature-controlled stage, an objective heater (Bioptechs), a 40X Plan-Neofluar objective lens (numerical aperture = 1.3). Fluorescent illumination was driven by an ultrahigh-speed wavelength switcher Lambda DG4 (Sutter Instrument) equipped with a 175 W xenon arc lamp and excitation filters for CFP and FRET (λex = 430 nm) and for YFP (λex = 505 nm) (Chroma Technology). Emission filters for CFP (λem = 470 nm), for YFP and FRET (λem = 535 nm) (Chroma Technology), were selected using a high-speed Lambda 10 filter wheel (Sutter Instrument), the microscope filter cube was equipped with a double-band CFP/YFP beamsplitter (86002bs, Chroma Technology). Images were acquired with a cooled, digital, charge-coupled device camera ($CoolSNAP_{HQ}$, Photometrics). All devices were controlled by MetaMorph Imaging System software (Universal Imaging).

Ratiometric imaging

Ratiometric imaging allows correction of YFP-actin fluorescence for path length. Fluorescence images, corresponding to CFP (I_C) and YFP (I_Y), were acquired every 20 s for 30 min with an exposure time of 100 ms for each image. For image processing, all fluorescent images were first corrected for shading and camera dark noise. A ratio image was obtained by dividing at corresponding pixels, the fluorescence intensities of the YFP image by the corresponding fluorescence intensities of the CFP image, and multiplying by 100.

FRET stoichiometry imaging

FRET occurs when an excited donor fluorophore (e.g. CFP) is located in close proximity (≤ 10 nm) to a lower-energy acceptor fluorophore (e.g. YFP). FRET stoichiometry is an analytical imaging method that can quantify FRET between separately expressed fluorescent proteins inside cells. Image acquisition and processing for FRET stoichiometry were performed as previously described (Hoppe *et al*., 2002). Three fluorescence images of a cell corresponding to CFP (I_D), YFP (I_A) and FRET (I_F), and a fourth phase-contrast image were acquired with an exposure time of 100 ms for each image. For image processing, fluorescence images were first corrected for shading and camera dark noise. FRET stoichiometry equations include the coefficients α, β, γ, ξ, that are characteristic of the microscope equipment and settings for a given FRET pair of fluorochromes. These coefficients were determined from Vero cells expressing YFP only (α = 0.142), CFP only (β = 0.643) and a linked CFP-YFP chimera (γ = 0.079 and ξ= 0.021). Image series were collected every 20 s for 30 min. No photobleaching was observed over the recording time of 30 min. Application of FRET stoichiometry equations to the acquired I_D, I_A and I_F images allowed the determination of E_A, E_D and R_M, using Metamorph software. For each pixel of the image, R_M (Eqn 1) represented the molar ratio of YFP to CFP. The apparent FRET efficiency, E_A (Eqn 2) was the fraction of YFP chimera in complex with CFP, times the characteristic FRET efficiency (E_c) of the YFP/CFP complex, and the apparent FRET efficiency E_D (Eqn 3) was the fraction of CFP chimera in complex with YFP, times the characteristic FRET efficiency (E_c) of the YFP/CFP complex.

$$R_M = \frac{[YFP]}{[CFP]} \quad (1)$$

$$E_A = \frac{E_c[C_{YFP\text{-}CFP}]}{[YFP]} \quad (2)$$

$$E_D = \frac{E_c[C_{YFP\text{-}CFP}]}{[CFP]} \quad (3)$$

FRET stoichiometry measurement between YFP-AktPH and CFP-AktPH as a readout of PI 3-kinase activation. Cells were co-transfected with plasmids encoding YFP-AktPH and CFP-AktPH. I_D, I_A and I_F images were collected every 20 s. Application of the FRET stoichiometry equations, pixel by pixel, to the I_A, I_D

and I_F images was used to create a new image in which each pixel corresponds to $(E_A + E_D)/2$; this term allows comparison of FRET signals from cells expressing different molar ratios of fluorescent proteins. For kinetic studies we calculated, for each cell and time point, the mean $(E_A + E_D)/2$ over the entire cell. At least 10 cells were recorded in each condition, and final kinetics were expressed as the mean $E_{AVE} = (E_A + E_D)/2 \pm$ SEM.

Determination of the fraction of active Rho-family GTPases. Cells were co-transfected with plasmids encoding YFP-Rac1 or YFP-Cdc42 and CFP-PBD. I_D, I_A and I_F images were collected every 20 s. Application of the FRET stoichiometry equations, pixel by pixel, to the acquired images (I_D, I_A and I_F) determined R_M, E_A and E_D for each pixel. To quantify and normalize the fraction of active GTPases (G) between cells expressing various molar ratios of fluorescent chimeras, E_A was divided by E_A^* ($G = E_A/E_A^*$). E_A^* is a coefficient calculated for each cell, that takes into account the characteristic FRET efficiency value (E_c) of the bimolecular complex YFP-Rac1/CFP-PBD. Images were rescaled according to the mean value of R_M. E_A^* was calculated as described (Hoppe and Swanson, 2004), using cells expressing various ratios of the constitutively active YFP-Rac1L61 and CFP-PBD. For kinetic studies we calculated, for each cell and time point, the mean G value over the entire cell image. At least 10 cells were analysed in each experimental condition, and each time point was expressed as the mean $G \pm$ SEM over the analysed cells.

Measurements of phosphoinositides

A total of 1.5×10^6 Vero cells were seeded in 75 cm^2 culture flasks and were grown in DMEM + 10% serum for 48 h. Cells were then incubated for 6 h in serum-free DMEM without phosphate (Sigma) containing 200 $\mu Ci\ ml^{-1}$ ^{32}Pi. For cholesterol-depleted cells the same protocol was followed except that MβCD (10 mM) was added to the flask for the last 30 min of incubation time. Cells were then washed and immediately incubated with phosphate-free DMEM containing 5.7 nM InlB for 2 min at room temperature. PI(3)P, PI(4)P, PI(3,4)P_2, PI(4,5)P_2 and PI(3,4,5)P_3 were quantified as previously described (Ireton *et al*., 1999). Briefly, cells were washed with cold phosphate-buffered saline (PBS), and 2.4 N HCl solution was added. Lipids were isolated and separated by thin-layer chromatography, then quantified by high-performance liquid chromatography (HPLC) system with a Whatman Partisphere SAX column.

Detection of phosphorylated Akt (Ser 473) by Western blotting experiments

A total of 0.5×10^6 Vero cells were seeded in 20 cm^2 culture flasks and were grown in DMEM + 10% serum for 48 h. Cells were then washed and incubated for 30 min in serum-free DMEM. Cells were then cholesterol-depleted for 30 min in DMEM containing MβCD (10 mM) or in DMEM (control cells). Cells were washed and immediately incubated in DMEM with or without InlB (1.25 nM) for 3, 10 and 20 min at 37°C. Cells were washed with cold PBS and lysis was performed in 800 µl of cold solubilization buffer [1% NP-40, 150 mM NaCl, 20 mM Tris/HCl pH 7.4, 2 mM EDTA, 3 mM sodium orthovanadate, 50 mM sodium fluoride, 1/100 cocktail inhibitors set III (Calbiochem)]. Cells lysates were subjected to Bradford protein assay (Sigma) and equal amounts of proteins were utilized for Western blotting experiments. Akt and Phospho-Akt (Ser 473) were detected using rabbit antiserum obtained from Cell Signaling.

Acknowledgements

This work received financial support from the Institut Pasteur (GPH 9) and ACI microbiologie. S. Seveau was supported by the Institut Pasteur (GPH 9). J.A.S and A.D.H. were supported by National Institutes of Health Grant AI35950.

References

Banerjee, M., Copp, J., Vuga, D., Marino, M., Chapman, T., van der Geer, P., and Ghosh, P. (2004) GW domains of the *Listeria monocytogenes* invasion protein InlB are required for potentiation of Met activation. *Mol Microbiol* **52:** 257–271.

Benard, V., Bohl, B.P., and Bokoch, G.M. (1999) Characterization of rac and cdc42 activation in chemoattractant-stimulated human neutrophils using a novel assay for active GTPases. *J Biol Chem* **274:** 13198–13204.

Bierne, H., and Cossart, P. (2002) InlB, a surface protein of *Listeria monocytogenes* that behaves as an invasin and a growth factor. *J Cell Sci* **115:** 3357–3367.

Bierne, H., Dramsi, S., Gratacap, M.P., Randriamampita, C., Carpenter, G., Payrastre, B., and Cossart, P. (2000) The invasion protein InlB from *Listeria monocytogenes* activates PLC-gamma1 downstream from PI 3-kinase. *Cell Microbiol* **2:** 465–476.

Bierne, H., Gouin, E., Roux, P., Caroni, P., Yin, H.L., and Cossart, P. (2001) A role for cofilin and LIM kinase in *Listeria*-induced phagocytosis. *J Cell Biol* **155:** 101–112.

Bierne, H., Miki, H., Innocenti, M., Scita, G., Gertler, F.B., Takenawa, T., and Cossart, P. (2005) WASP-related proteins, Abi1 and Ena/VASP are required for *Listeria* invasion induced by the Met receptor. *J Cell Sci* **118:** 1537–1547.

Birchmeier, C., and Gherardi, E. (1998) Developmental roles of HGF/SF and its receptor, the c-Met tyrosine kinase. *Trends Cell Biol* **8:** 404–410.

Bodin, S., Giuriato, S., Ragab, J., Humbel, B.M., Viala, C., Vieu, C., *et al.* (2001) Production of phosphatidylinositol 3,4,5-trisphosphate and phosphatidic acid in platelet rafts: evidence for a critical role of cholesterol-enriched domains in human platelet activation. *Biochemistry* **40:** 15290–15299.

Braun, L., Ohayon, H., and Cossart, P. (1998) The InlB protein of *Listeria monocytogenes* is sufficient to promote entry into mammalian cells. *Mol Microbiol* **27:** 1077–1087.

Braun, L., Nato, F., Payrastre, B., Mazie, J.C., and Cossart, P. (1999) The 213-amino-acid leucine-rich repeat region of the *Listeria monocytogenes* InlB protein is sufficient for entry into mammalian cells, stimulation of PI 3-kinase and membrane ruffling. *Mol Microbiol* **34:** 10–23.

Copp, J., Marino, M., Banerjee, M., Ghosh, P., and van der Geer, P. (2003) Multiple regions of internalin B contribute to its ability to turn on the Ras-mitogen-activated protein kinase pathway. *J Biol Chem* **278:** 7783–7789.

Cossart, P., and Sansonetti, P.J. (2004) Bacterial invasion: the paradigms of enteroinvasive pathogens. *Science* **304:** 242–248.

Dramsi, S., and Cossart, P. (2003) Listeriolysin O-mediated calcium influx potentiates entry of *Listeria monocytogenes* into the human Hep-2 epithelial cell line. *Infect Immun* **71:** 3614–3618.

Dramsi, S., Biswas, I., Maguin, E., Braun, L., Mastroeni, P., and Cossart, P. (1995) Entry of *Listeria monocytogenes* into hepatocytes requires expression of inlB, a surface protein of the internalin multigene family. *Mol Microbiol* **16:** 251–261.

Fujitani, M., Honda, A., Hata, K., Yamagishi, S., Tohyama, M., and Yamashita, T. (2005) Biological activity of neurotrophins is dependent on recruitment of Rac1 to lipid rafts. *Biochem Biophys Res Commun* **327:** 150–154.

Gekara, N.O., Jacobs, T., Chakraborty, T., and Weiss, S. (2005) The cholesterol-dependent cytolysin listeriolysin O aggregates rafts via oligomerization. *Cell Microbiol* **7:** 1345–1356.

Genot, E.M., Arrieumerlou, C., Ku, G., Burgering, B.M., Weiss, A., and Kramer, I.M. (2000) The T-cell receptor regulates Akt (protein kinase B) via a pathway involving Rac1 and phosphatidylinositide 3-kinase. *Mol Cell Biol* **20:** 5469–5478.

Golub, T., Wacha, S., and Caroni, P. (2004) Spatial and temporal control of signaling through lipid rafts. *Curr Opin Neurobiol* **14:** 542–550.

Haugh, J.M., Codazzi, F., Teruel, M., and Meyer, T. (2000) Spatial sensing in fibroblasts mediated by 3′ phosphoinositides. *J Cell Biology* **151:** 1269–1280.

Henry, R.M., Hoppe, A.D., Joshi, N., and Swanson, J.A. (2004) The uniformity of phagosome maturation in macrophages. *J Cell Biol* **164:** 185–194.

Hoppe, A., Christensen, K., and Swanson, J.A. (2002) Fluorescence resonance energy transfer-based stoichiometry in living cells. *Biophys J* **83:** 3652–3664.

Hoppe, A.D., and Swanson, J.A. (2004) Cdc42, Rac1, and Rac2 display distinct patterns of activation during phagocytosis. *Mol Biol Cell* **15:** 3509–3519.

Ireton, K., Payrastre, B., and Cossart, P. (1999) The *Listeria monocytogenes* protein InlB is an agonist of mammalian phosphoinositide 3-kinase. *J Biol Chem* **274:** 17025–17032.

Jonquieres, R., Pizarro-Cerda, J., and Cossart, P. (2001) Synergy between the N- and C-terminal domains of InlB for efficient invasion of non-phagocytic cells by *Listeria monocytogenes*. *Mol Microbiol* **42:** 955–965.

Kiyokawa, E., Hashimoto, Y., Kobayashi, S., Sugimura, H., Kurata, T., and Matsuda, M. (1998) Activation of Rac1 by a Crk SH3-binding protein, DOCK180. *Genes Dev* **12:** 3331–3336.

Lecuit, M., Vandormael-Pournin, S., Lefort, J., Huerre, M., Gounon, P., Dupuy, C., *et al.* (2001) A transgenic model for listeriosis: role of internalin in crossing the intestinal barrier. *Science* **292:** 1722–1725.

Li, N., Xiang, G.S., Dokainish, H., Ireton, K., and Elferink, L.A. (2005) The *Listeria* protein internalin B mimics hepatocyte growth factor-induced receptor trafficking. *Traffic* **6:** 459–473.

Osaki, M., Oshimura, M., and Ito, H. (2004) PI3K-Akt pathway: its functions and alterations in human cancer. *Apoptosis* **9:** 667–676.

Pierini, L.M., Eddy, R.J., Fuortes, M., Seveau, S., Casulo, C., and Maxfield, F.R. (2003) Membrane lipid organization is critical for human neutrophil polarization. *J Biol Chem* **278:** 10831–10841.

del Pozo, M.A., Alderson, N.B., Kiosses, W.B., Chiang, H.H., Anderson, R.G., and Schwartz, M.A. (2004) Integrins regulate Rac targeting by internalization of membrane domains. [See comment]. *Science* **303:** 839–842.

Rajendran, L., and Simons, K. (2005) Lipid rafts and membrane dynamics. *J Cell Sci* **118:** 1099–1102.

Royal, I., Lamarche-Vane, N., Lamorte, L., Kaibuchi, K., and Park, M. (2000) Activation of cdc42, rac, PAK, and rho-kinase in response to hepatocyte growth factor differentially regulates epithelial cell colony spreading and dissociation. *Mol Biol Cell* **11:** 1709–1725.

Santos, O.F., Barros, E.J., Yang, X.M., Matsumoto, K., Nakamura, T., Park, M., and Nigam, S.K. (1994) Involvement of hepatocyte growth factor in kidney development. *Dev Biol* **163:** 525–529.

Schmidt, C., Bladt, F., Goedecke, S., Brinkmann, V., Zschiesche, W., Sharpe, M., *et al.* (1995) Scatter factor/hepatocyte growth factor is essential for liver development. *Nature* **373:** 699–702.

Seveau, S., Bierne, H., Giroux, S., Prevost, M.C., and Cossart, P. (2004) Role of lipid rafts in E-cadherin- and HGF-R/Met-mediated entry of *Listeria monocytogenes* into host cells. *J Cell Biol* **166:** 743–753.

Shen, Y., Naujokas, M., Park, M., and Ireton, K. (2000) InlB-dependent internalization of *Listeria* is mediated by the Met receptor tyrosine kinase. *Cell* **103:** 501–510.

Sun, H., Shen, Y., Dokainish, H., Holgado-Madruga, M., Wong, A., and Ireton, K. (2005) Host adaptor proteins Gab1 and CrkII promote InlB-dependent entry of *Listeria monocytogenes*. *Cell Microbiol* **7:** 443–457.

Vanhaesebroeck, B., and Alessi, D.R. (2000) The PI3K-PDK1 connection: more than just a road to PKB. *Biochem J* **346** (Part 3)**:** 561–576.

Vazquez-Boland, J.A., Kuhn, M., Berche, P., Chakraborty, T., Dominguez-Bernal, G., Goebel, W., *et al.* (2001) *Listeria* pathogenesis and molecular virulence determinants. *Clin Microbiol Rev* **14:** 584–640.

Veiga, E., and Cossart, P. (2005) *Listeria* hijacks the clathrin-dependent endocytic machinery to invade mammalian cells. *Nat Cell Biol* **7:** 894–900.

Wysoczynski, M., Reca, R., Ratajczak, J., Kucia, M., Shirvaikar, N., Honczarenko, M., *et al.* (2005) Incorporation of CXCR4 into membrane lipid raft primes noming-related responses of hematopoietic stem/progenitor cells to an SDF-1 gradient. *Blood* **105:** 40–48.

Zacharias, D.A., Violin, J.D., Newton, A.C., and Tsien, R.Y. (2002) Partitioning of lipid-modified monomeric GFPs into membrane microdomains of live cells. *Science* **296:** 913–916.

Supplementary material

The following supplementary material is available for this article online:

Fig. S1. Transiently transfected Vero cells were placed on the microscope stage at 37°C and image series were collected every 20 s for 30 min. InlB or HGF was added 4.5 min after the start of imaging. Collected images (phase-contrast, I_A, I_D, I_F) and a processed FRET image, in which each pixel represents the average ($E_A + E_D$)/2 value of a cell expressing YFP-AktPH plus CFP-AktPH, after 4.5 min of stimulation by 1.25 nM InlB.

Fig. S2. Transiently transfected Vero cells were placed on the microscope stage at 37°C and image series were collected every 20 s for 30 min. For the stimulated cells, 5.7 nM InlB was added 4.5 min after the start of imaging. Collected images (phase-contrast, I_A, I_D, I_F) and processed FRET image (G), of a cell expressing YFP-Rac1 plus CFP-PBD, after 1 min of stimulation with InlB.

Fig. S3. Vero cells were pre-incubated with ^{32}Pi, and were cholesterol-depleted, or not (–), with 10 mM MβCD. After washes, cells were stimulated, or not (NS), with InlB for 2 min at room temperature. Phosphoinositides were then isolated and quantified by HPLC as described in *Experimental procedures*. Results were normalized according to the total amount of phospholipids present in each sample. Average ± SEM of two independent experiments are presented in cpm.

Movie 1. Vero cells expressing YFP-AktPH plus CFP-AktPH were incubated with a *L. innocua* expressing InlB. Phase-contrast and fluorescence images (I_A, I_D, I_F) were collected every 20 s for 30 min. Movie 1A shows phase-contrast (top left), FRET (I_F, top right), AktPH-CFP (I_D, bottom left) and AktPH-YFP (I_A, bottom right) images. Movie 1B shows the processed FRET images. Movies are 200 times accelerated. Scale bar = 20 μm. Time is indicated in s.

Movie 2. Vero cells expressing YFP-Rac1 plus CFP-PBD were incubated with a *L. innocua* expressing InlB. Phase-contrast and fluorescence images (I_A, I_D, I_F) were collected every 20 s for 30 min. Movie 2A shows phase-contrast (top left), FRET (I_F, top right), PBD-CFP (I_D, bottom left) and YFP-Rac1 (I_A, bottom right) images. Movie 2B shows the processed FRET images. Movies are 200 times accelerated. Scale bar = 20 μm. Time is indicated in s.

Movie 3. Vero cells expressing CFP plus YFP-actin were stimulated with InlB (1.25 nM) or HGF (1.25 nM) 3 min after the start of imaging (T_0). Phase-contrast and fluorescence images (I_Y, I_C) were recorded every 20 s for 30 min. Movies 3A and B show phase-contrast (top left), Ratio (top right), YFP (bottom left) and CFP (bottom right) images of cells stimulated with InlB or HGF respectively. Movies are 200 times accelerated. Scale bar = 20 μm. Time is indicated in s.

Movie 4. Images of Vero cells expressing YFP-AktPH plus CFP-AktPH were collected every 20 s for 30 min. Movie 4A shows phase-contrast and fluorescence images (I_A, I_D, I_F) of a cell stimulated with 1.25 nM InlB (at time = 270 s). Movie 4B shows the corresponding processed FRET images. Movie 4C shows processed FRET images of an unstimulated cell (left panel) and of a cell stimulated with 1.25 nM of HGF (right panel). Movies are 200 times accelerated. Scale bar = 20 μm. Time is indicated in s.

Movie 5. Transiently transfected Vero cells were placed on the microscope stage at 37°C and image series were collected every 20 s for 30 min. Cells were stimulated with 5.7 nM InlB 4.5 min after the start of imaging. Movie 5A shows the collected images (phase-contrast, I_A, I_D, I_F) of a cell expressing YFP-Rac1 plus CFP-PBD and Movie 5B shows the corresponding processed FRET images (Ratio, E_A and E_D). Movie 5C shows Vero cells expressing YFP-Rac1L61 plus CFP-PBD (left panel) and YFP-Rac1 plus CFP-PBD (right panel). Movies are 200 times accelerated. Scale bar = 20 μm. Time is indicated in s.

This material is available as part of the online article from http://www.blackwell-synergy.com